

Transformations of low-angle tilt boundaries in high- T_c superconductors

M. Yu. Gutkin and I. A. Ovid'ko*

Institute of Problems of Mechanical Engineering, Russian Academy of Sciences, Bolshoj 61, Vasilievskij Ostrov, 199178 St. Petersburg, Russia

(Received 4 April 2000; published 23 January 2001)

Theoretical models are suggested which describe the transformations of low-angle tilt boundaries in high- T_c superconductors. Conditions are theoretically revealed at which the formation of split and amorphous dislocation configurations in low-angle tilt boundaries is energetically favorable. The results of the suggested models account for experimental data [M. F. Chisholm and D. A. Smith, *Philos. Mag. A* **59**, 181 (1989)] on observation of low-angle tilt boundaries consisting of either split or amorphous dislocation configurations in high- T_c superconductors.

DOI: 10.1103/PhysRevB.63.064515

PACS number(s): 74.80.Dm, 74.20.De, 74.60.Jg

I. INTRODUCTION

The critical current density in polycrystalline high- T_c superconductors is strongly suppressed by grain boundaries; e.g., see Refs. 2–7. The grain-boundary effect in question, on the one hand, plaques high-current applications of polycrystalline superconducting materials and, on the other hand, is interesting for understanding the fundamentals of high- T_c superconductivity. Several physical mechanisms have been proposed as those causing the drastic reduction of the critical current density across grain boundaries.^{8–18} So, suppression of the transport properties of grain boundaries is attributed to the following factors: (i) structural disorder within cores of grain boundaries;^{8–10} (ii) structural disorder induced by stress fields of grain-boundary dislocations;^{8–10,17} (iii) deviations from bulk stoichiometry in vicinities of grain boundaries;^{11,12,18} (iv) band bending;^{9,14–16} (v) the combined effects of d -wave-type symmetry of the superconducting order parameter and the faceted microstructure of grain boundaries.¹³ However, a systematic understanding of the grain-boundary effect on high- T_c superconductivity is still expected (e.g., see reviews, Refs. 6, 7, and 19).

The most remarkable experimentally documented fact in the area discussed is the general disparity between the behavior of low- and high-angle boundaries.^{2–7} So, the critical current density J_c across low-angle boundaries drastically decreases with boundary misorientation θ tentatively as: $J_c(\theta) \approx J_c(0^\circ) \exp(-\theta/8^\circ)$, where θ ranges from 0° to about 15° . High-angle boundaries are characterized by low values of $J_c(\theta) \approx (10^{-3} - 10^{-2}) J_c(0^\circ)$, which are weakly sensitive to boundary misorientation $\theta (> 15^\circ)$. In order to explain the low-angle/high-angle distinction as well as the associated experimental data on the grain-boundary effect on high- T_c superconductivity, theoretical models^{8–10,17} have been proposed treating the effect as that related to suppression of the superconducting order parameter within crystallographically disordered cores of grain boundaries and their elastically stressed vicinities. These models view geometric parameters of grain-boundary cores and distributions of grain-boundary-induced stress fields as the very important factors strongly affecting the critical current density J_c across grain boundaries in high- T_c superconductors. Also, characteristics of core regions and stress fields of grain boundaries essentially

influence the local oxygen concentration and the electric charge density inhomogeneities which, according to models,^{9,12,18} are capable of causing the superconducting order-parameter modification close to grain boundaries and their transport properties. In this context, an analysis of transformations of core regions and stress fields of grain boundaries is of primary interest for a description of the grain-boundary effect on high- T_c superconductivity. The main aim of this paper is to propose theoretical models which describe the experimentally observed¹ formation of split and amorphized dislocations (Fig. 1) composing low-angle boundaries in high- T_c superconductors.

As it has been revealed in the experiments,¹ the structure of low-angle [100] tilt boundaries in $\text{YBa}_2\text{Cu}_3\text{O}_{7-\delta}$ superconductors drastically changes with boundary misorientation θ . So, for $\theta \approx 5^\circ$, tilt boundaries represent walls of split dislocation configurations each consisting of three partial dislocations of the edge type [Fig. 1(b)]. The sum Burgers vector of a split dislocation configuration is the crystal lattice vector $\mathbf{B} = (0,0,B)$ in conventional (a, b, c) crystallography of high- T_c superconducting cuprates, where $B \approx 1.17$ nm. Each partial dislocation composing a split dislocation configuration [Fig. 1(b)] is characterized by Burgers vector $\mathbf{b} = (0,0,b)$

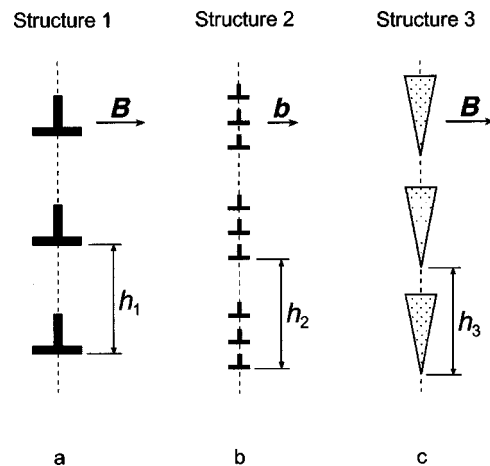


FIG. 1. Structures of low-angle tilt boundaries in high- T_c superconductors: (a) conventional, (b) split, and (c) amorphous structures.

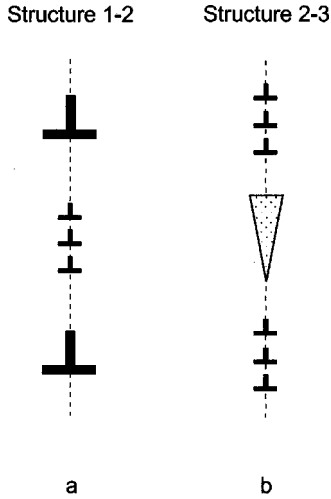


FIG. 2. Wall of perfect dislocations with one dislocation being replaced by a split dislocation configuration (low-angle boundary structure 1-2) (a), and wall of split dislocation configurations with one split dislocation configuration being replaced by an amorphous dislocation configuration (low-angle boundary structure 2-3) (b).

with b being equal to $B/3$. The neighboring partial dislocations in the boundary with $\theta \approx 5^\circ$ are distant by tentatively $12b$.

Low-angle $[100]$ tilt boundaries with $\theta \approx 7^\circ$ represent walls of dislocation configurations with amorphous cores having triangle-like sections¹ [Fig. 1(c)]. Such ‘‘amorphous’’ dislocation configurations as elements of low-angle boundaries provide misorientation of adjacent crystalline grains in $\text{YBa}_2\text{Cu}_3\text{O}_{7-\delta}$ superconductors and are characterized by Burgers vectors of the $(0,0,B)$ type.¹

In order to theoretically characterize the conditions at which the structural transformations of low-angle tilt boundaries occur in high- T_c superconductors, we will distinguish the three basic structures of such boundaries: conventional [Fig. 1(a)], ‘‘split’’ [Fig. 1(b)], and ‘‘amorphous’’ [Fig. 1(c)] structures. A tilt boundary with the conventional structure represents a wall of periodically spaced (with period h_1) perfect dislocations with Burgers vectors of the $(0,0,B)$ type [Fig. 1(a)]. The split structure of a low-angle tilt boundary [see Fig. 1(b)] corresponds to a wall of periodically arranged (with period h_2) split dislocation configurations [Fig. 1(b)]. A tilt boundary with the amorphous structure is modeled as a wall of periodically arranged (with period h_3) amorphous dislocation configurations [Fig. 1(c)]. For purposes of this paper dealing with a theoretical description of the structural transformations of low-angle tilt boundaries in high- T_c superconductors, we will focus on the situation with elements of the split and amorphous structures being generated in the pre-existent, respectively conventional, and split, structures of a low-angle tilt boundary. In other words, we will theoretically examine characteristics of the two new dislocation structures: a wall of perfect dislocations with one perfect dislocation being replaced by a split dislocation configuration [Fig. 2(a)] and a wall of split dislocation configurations with one split configuration being replaced by an amorphous dislocation configuration [Fig. 2(b)]. In these circumstances,

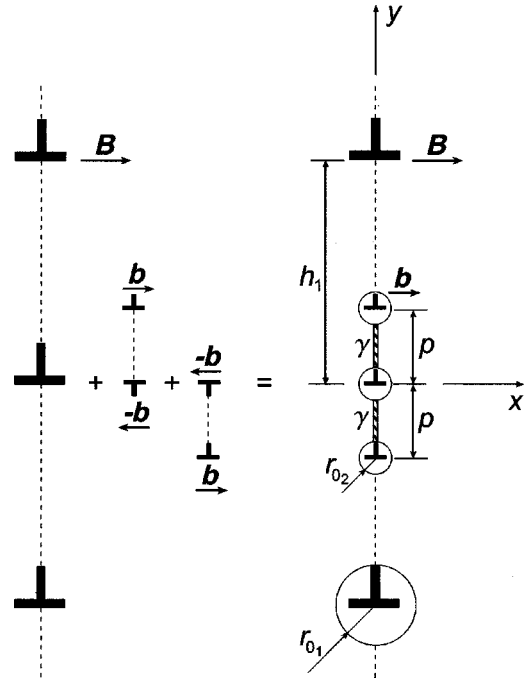


FIG. 3. Split dislocation configuration is represented as a perfect dislocation and two dipoles of partial dislocations.

in order to quantitatively describe the conditions at which the structural transformations in question occur, we will examine the conditions at which the formation of the new dislocation structures (Fig. 2) is energetically favorable.

II. GENERATION OF A SPLIT DISLOCATION CONFIGURATION IN CONVENTIONAL LOW-ANGLE TILT BOUNDARY

Let us consider a wall of perfect dislocations with one perfect dislocation being replaced by a split dislocation configuration [Fig. 2(a)]. Following the theory of dislocations in solids,²⁰ the split dislocation configuration can be represented as a perfect dislocation and two dipoles of partial dislocations as shown in Fig. 3. In the framework of this representation, the lower dislocation of the top dipole and the top dislocation of the lower dipole are located at the same position as the perfect dislocation, in which case their combination is equivalent to one partial dislocation, the dislocation in the center of the split configuration shown in Fig. 3.

With the representation (Fig. 3) taken into account, let us consider the difference in the energy (per unit length of dislocations) between the conventional dislocation wall [Fig. 1(a)] and the dislocation structure shown in Fig. 2(a). (For simplicity, hereinafter, the conventional dislocation structure [Fig. 1(a)] and the dislocation structure shown in Fig. 2(a) will be denoted as structure 1 and structure 1-2, respectively.) The energy of structure 1 can be written as follows:

$$W_1 = RW_1^{el} + \frac{R}{h_1} W_1^c, \quad (1)$$

where R denotes the length of a tilt boundary modeled as structure 1, W_1^{el} the elastic energy density of structure 1 per its unit length, and W_1^c the energy of a perfect (nonsplit) dislocation core.

The energy of structure 1-2 is given as

$$W_{1-2} = RW_1^{el} + \left(\frac{R}{h_1} - 1\right) W_1^c + 2W_{dip}^{el} + 3W_2^c + W_{int}^{dip} + 2W_{int}^{dip-b1} + 2(p - 2r_{0_2})\gamma. \quad (2)$$

Here W_{dip}^{el} denotes the proper energy of a dipole of partial dislocations, W_2^c the energy of a partial dislocation core, W_{int}^{dip} the energy of interaction between the dipoles (Fig. 3), W_{int}^{dip-b1} the energy of interaction between a dipole of partial dislocations and structure 1, r_{0_2} the radius of a partial dislocation core, γ the energy of stacking fault formed between the partial dislocations composing the split dislocation configuration (Fig. 3).

From Eqs. (1) and (2) we find that the change in the energy, that accompanies transformation of structure 1 into structure 1-2, is as follows:

$$\begin{aligned} \Delta W_{1-2} &= W_{1-2} - W_1 \\ &= -W_1^c + 2W_{dip}^{el} + 3W_2^c + W_{int}^{dip} \\ &\quad + 2W_{int}^{dip-b1} + 2(p - 2r_{0_2})\gamma. \end{aligned} \quad (3)$$

The equation $\Delta W_{1-2} = 0$ corresponds to the critical conditions at which the structure-1-to-structure-1-2 transformation occurs.

Let us consider terms on the right-hand side (rhs) of formula (3). The dislocation core energy for a perfect dislocation (W_1^c) and a partial dislocation (W_2^c) are given by the known formula²⁰

$$W_i^c = \frac{Gb_i^2 Z_i}{4\pi(1-\nu)}, \quad (4)$$

with Z_i being a nondimensional constant of the order of 1; $i=1,2$; $b_1=B$; $b_2=b$; G denotes the shear modulus and ν the Poisson ratio. According to the general calculation scheme,²⁰ the proper energy of a dipole of partial dislocations is calculated as the work spent to the generation of the dipole in its stress field $\sigma_{xx}^{dip}(x=0,y)$:

$$\begin{aligned} W_{dip}^{el} &= \frac{b}{2} \int_{r_{0_2}}^{p-r_{0_2}} \sigma_{xx}^{dip}(x=0,y) dy \\ &= -\frac{Gb^2}{4\pi(1-\nu)} \int_{r_{0_2}}^{p-r_{0_2}} \left(\frac{1}{y-p} - \frac{1}{y}\right) dy \\ &= \frac{Gb^2}{2\pi(1-\nu)} \ln \frac{p-r_{0_2}}{r_{0_2}}. \end{aligned} \quad (5)$$

Both the energy of the dipole-dipole interaction and that of the dipole-structure-1 interaction are calculated in the same

way in the framework of the scheme.²⁰ So, the former energy W_{int}^{dip} is calculated as the work spent to the generation of one dipole in the stress field created by another dipole of partial dislocations:

$$\begin{aligned} W_{int}^{dip} &= b \int_{r_{0_2}}^p \sigma_{xx}^{dip}(x=0,y) dy \\ &= \frac{Gb^2}{2\pi(1-\nu)} \int_{r_{0_2}}^p \left(\frac{1}{y+p} - \frac{1}{y}\right) dy \\ &= -\frac{Gb^2}{2\pi(1-\nu)} \ln \frac{p+r_{0_2}}{2r_{0_2}}. \end{aligned} \quad (6)$$

The energy of the dipole-structure-1 interaction W_{int}^{dip-b1} is calculated as the work spent to the generation of the dipole in the structure-1-induced stress field which is given as²⁰

$$\sigma_{xx}^{b1}(x,y) = -\frac{GB \sin \bar{y} (\cosh \bar{x} - \cos \bar{y} + \bar{x} \sinh \bar{x})}{2(1-\nu)h_1 (\cosh \bar{x} - \cos \bar{y})^2}. \quad (7)$$

Here $\bar{x} = 2\pi x/h_1$; $\bar{y} = 2\pi y/h_1$; $\bar{p} = 2\pi p/h_1$. In these circumstances, we find the energy W_{int}^{dip-b1} as

$$\begin{aligned} W_{int}^{dip-b1} &= b \int_{r_{0_1}}^p \sigma_{xx}^{b1}(x=0,y) dy \\ &= -\frac{GBb}{4\pi(1-\nu)} \ln \frac{1 - \cos \bar{p}}{1 - \cos \bar{r}_{0_1}}, \end{aligned} \quad (8)$$

where r_{0_1} is the radius of a perfect dislocation core.

With Eqs. (4)–(6) and (8) substituted to Eq. (3), we have

$$\begin{aligned} \Delta W_{1-2} &= \frac{Gb^2}{4\pi(1-\nu)} \left(3Z_2 - \frac{B^2}{b^2} Z_1 + 2 \ln \frac{2(p-r_{0_2})}{r_{0_2}(p+r_{0_2})} \right. \\ &\quad \left. - 2 \frac{B}{b} \ln \frac{1 - \cos \bar{p}}{1 - \cos \bar{r}_{0_1}} \right) + 2(p - 2r_{0_2})\gamma. \end{aligned} \quad (9)$$

Following estimates of Ref. 1, the stacking fault energy γ figuring on the rhs of Eq. (9) is approximately given as $\gamma \approx 7GB/[324\pi(1-\nu)]$. With this taken into consideration, we numerically calculated with the help of formula (9) the dependence of ΔW_{1-2} on boundary misorientation θ [which is in the following Frank's relationship²⁰ with parameters of the dislocation structures: $B = 2h_1 \sin(\theta/2)$], for characteristic values of parameters: $B = 3b$, $Z_1 \approx Z_2 \approx 1$, $r_{0_1} \approx B$, and $r_{0_2} \approx b$ (see Fig. 3). According to the results of these calculations, the energy change ΔW_{1-2} is negative in the range of θ from 0° to 7° , for $2b \leq p \leq 17b$. As a corollary, the existence of low-angle boundaries (with $\theta \leq 7^\circ$) consisting of split dislocation configurations [Fig. 1(b)] is more energetically favorable than that of low-angle boundaries consisting of perfect dislocations [Fig. 1(a)]. Also, our calculations indicate that the so-called equilibrium distance p_{eq} between neighboring partial dislocations (that is, the distance corre-

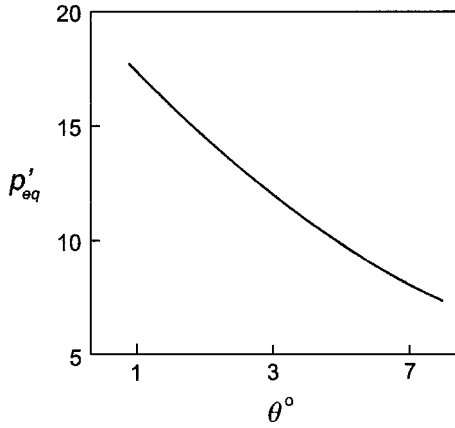


FIG. 4. Dependence of equilibrium distance $p'_{eq} = p_{eq}/b$ between neighboring partial dislocations in a split configuration on tilt boundary misorientation angle θ .

sponding to the largest value of $|\Delta W_{1-2}|$, the difference in the energy density between structure 1 [Fig. 1(a)] and structure 1-2 [Fig. 2(a)] decreases with boundary misorientation θ (Fig. 4). For $\theta = 5^\circ$, from our calculations it follows that $p_{eq} \approx 11b$. This is in agreement with the experimentally measured¹ value ($\approx 12b$) of the distance between neighboring partial dislocations composing split dislocation configurations at $\theta = 5^\circ$.

III. GENERATION OF AN AMORPHOUS DISLOCATION CONFIGURATION IN WALL OF SPLIT DISLOCATION CONFIGURATIONS

Let us consider the transformation of the low-angle boundary structure composed of split dislocation configurations [Fig. 1(b)] into the structure composed of amorphous dislocation configurations [Fig. 1(c)]. (For simplicity, hereinafter, these structures will be denoted as structure 2 and structure 3, respectively.) To do so, by analogy with our consideration given in the previous section, we will focus on the ‘‘intermediate’’ structure, that is, a wall of split dislocation configurations with one split configuration being replaced by an amorphous dislocation configuration [Fig. 2(b)]. (Hereinafter, the structure under consideration will be denoted as structure 2-3.) More precisely, in order to quantitatively describe the conditions at which the transformation from structure 2 into structure 3 occurs, we will calculate the difference ΔW_{2-3} in the energy between structure 2 and structure 2-3.

The amorphous dislocation configuration has the amorphous core (with a triangle-like section) and is characterized by Burgers vector of the $(0,0,B)$ type. The amorphous dislocation core does not contain any experimentally distinguished, grain boundary or lattice, elemental dislocation(s).¹ In these circumstances, following the general model description of dislocations and grain boundaries with amorphous cores,²¹ the amorphous dislocation configuration [Fig. 1(c)] can be effectively represented as the amorphous core region with the dislocation charge—Burgers vector—continuously distributed at the boundary between the amorphous phase (the core of the amorphous dislocation configuration) and the

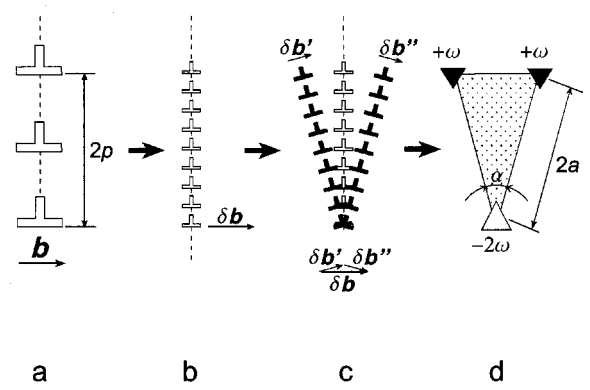


FIG. 5. Transformation of split dislocation configuration into amorphous dislocation configuration (model).

adjacent crystalline phase. With this representation taken into consideration, the amorphous dislocation configuration [Fig. 1(c)] is modeled as that resulted from the two splitting processes which are as follows: (i) the splitting of a split dislocation configuration [Fig. 5(a)] into a ragged wall of dislocations distributed continuously along the wall [Fig. 5(b)] and characterized by infinitesimally small Burgers vectors δb ; and (ii) the consequent splitting of the ragged wall into the two walls of continuously distributed elemental dislocations at the crystal/glass interphase boundary [Fig. 5(c)], characterized by Burgers vectors $\delta b'$ and $\delta b''$, in which case the walls are divided by the amorphous phase. The sum Burgers vector of the elemental dislocations [Fig. 5(c)] is $\mathbf{B} = (0,0,B)$.

The two ragged walls of the continuously distributed dislocations [Fig. 5(c)] create stress fields which are equivalent to those generated by the two dipoles of wedge disclinations shown in Fig. 5(d). The two disclinations (each is characterized by negative strength $-\omega$) that are the elements of the dipoles are located at the lower edge of the amorphous dislocation core [Fig. 5(d)] and, in fact, converge into one disclination characterized by strength -2ω . Two other disclinations (each being characterized by positive strength $+\omega$) are located at the upper edges of the amorphous dislocation core with section assumed to be an isosceles triangle [Fig. 5(d)]. The dipole arms are equal to the ragged wall length $2a$. The disclination strength ω is assumed to be small; for geometric reasons, $B \approx 4a\omega$,²² in which case we find $\omega \approx 3b/(4a)$.

In the framework of the model considered, we will analyze energetic characteristics of the formation of the disclination configuration [associated with the amorphous core, see Fig. 5(d)] in the wall of split dislocation configurations [Fig. 2(b)]. The ‘‘intermediate’’ structure 2-3 [Fig. 2(b)] can be represented as structure 2 combined with the two defect configurations: a virtual split dislocation configuration characterized by Burgers vector, $-\mathbf{B}$, and the disclination configuration with the amorphous core (Fig. 6). With this representation, the total energy (per unit length of dislocation configurations) of structure 2-3 can be written as follows:

$$W_{2-3} = W_2 - 3W_2^c + 3W_v^{el} + W_{int}^{vd-b2} + 2W_s^\Delta + W_{int}^\Delta + 2W_{int}^{\Delta-b2} + 2W_{int}^{\Delta-ud} + W_{am} + \Gamma_{a/c} - 2(p - 2r_0_2)\gamma, \quad (10)$$

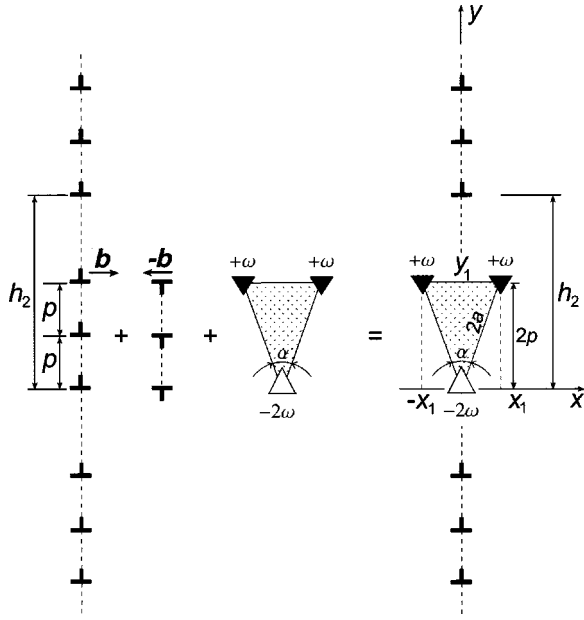


FIG. 6. Representation of an amorphous dislocation configuration as that resulted from the annihilation of a real split dislocation configuration with a virtual split dislocation configuration of opposite sign and the adding of the amorphous dislocation configuration.

where W_2 denotes the total energy of structure 2, the periodic wall of split dislocation configurations [Fig. 1(b)]; W_v^{el} the proper energy of a virtual dislocation with the Burgers vector $-\mathbf{B}/3$; W_{int}^{vd-b2} the energy of the interaction between the virtual split dislocation configuration and the structure 2; W_s^Δ the proper energy of a disclination dipole (composing the disclination configuration shown in Fig. 6); W_{int}^Δ the energy of the interaction between the disclination dipoles; $W_{int}^{\Delta-b2}$ the energy of the interaction between a disclination dipoles and structure 2; $W_{int}^{\Delta-vd}$ the energy of the interaction between a disclination dipole and the virtual split dislocation configuration; W_{am} the difference in the energy between the amorphous and crystalline phases; $\Gamma_{a/c}$ the surface energy of the interface between the amorphous and crystalline phases.

The transformation of structure 2 into the intermediate structure 2-3 is accompanied by the following change of the energy:

$$\begin{aligned} \Delta W_{2-3} &= W_{2-3} - W_2 \\ &= -3W_2^c + 3W_v^{el} + W_{int}^{vd-b2} + 2W_s^\Delta + W_{int}^\Delta + 2W_{int}^{\Delta-b2} \\ &\quad + 2W_{int}^{\Delta-vd} + W_{am} + \Gamma_{a/c} - 2(p - 2r_{0_2})\gamma. \end{aligned} \quad (11)$$

The equation $\Delta W_{2-3} = 0$ gives critical conditions at which the transformation occurs.

Let us analyze constituents of ΔW_{2-3} , figuring on the rhs of Eq. (11). The proper energy W_v^{el} of a virtual dislocation is given by the formula²⁰

$$W_v^{el} = \frac{Gb^2}{4\pi(1-\nu)} \ln \frac{R}{r_{0_2}}. \quad (12)$$

The energy W_{int}^{vd-b2} of the interaction between the virtual split dislocation configuration and structure 2 is calculated as the work spent to the generation of the configuration in the stress field σ_{xy}^{b2} of structure 2 when the virtual dislocations are introduced by gliding along planes $y=0$, $y=p$, and $y=2p$ from the closest outer boundary of the solid to the grain-boundary plane:

$$\begin{aligned} W_{int}^{vd-b2} &= -b \int_{r_{0_2}}^R \{ \sigma_{xy}^{b2}(x, y=0) + \sigma_{xy}^{b2}(x, y=p) \\ &\quad + \sigma_{xy}^{b2}(x, y=2p) \} dx. \end{aligned} \quad (13)$$

The stress field $\sigma_{xy}^{b2}(x, y)$ on the rhs of formula (13) represents the superposition of the stress fields σ_{xy} ,²⁰ induced by the three walls of edge dislocations with Burgers vectors \mathbf{b} , that are characterized by period h_2 and are shifted relative to each other by distances p and $2p$, respectively (Fig. 6):

$$\sigma_{xy}^{b2}(x, y) = \sigma_{xy}(x, y) + \sigma_{xy}(x, y-p) + \sigma_{xy}(x, y-2p), \quad (14)$$

$$\sigma_{xy}(x, y) = \frac{Gb\bar{x}(\cosh \bar{x} \cos \bar{y} - 1)}{2(1-\nu)h_2(\cosh \bar{x} - \cos \bar{y})^2}, \quad (15)$$

where $\bar{x} = 2\pi x/h_2$ and $\bar{y} = 2\pi y/h_2$. With Eqs. (14) and (15) substituted to Eq. (13), we have

$$\begin{aligned} W_{int}^{vd-b2} &= -\frac{Gb^2}{2\pi(1-\nu)} \{ 3[\eta_0 \coth \eta_0 - \ln(2 \sinh \eta_0)] \\ &\quad + 2\Phi(\eta_0, \bar{p}) + \Phi(\eta_0, 2\bar{p}) \}, \end{aligned} \quad (16)$$

where $\eta_0 = \pi r_{0_2}/h_2$, and

$$\Phi(\eta_0, t) = \frac{1}{4} \int_{2\eta_0}^{+\infty} \frac{\cosh x \cos t - 1}{(\cosh x - \cos t)^2} x dx. \quad (17)$$

The proper energy of the disclination dipole W_s^Δ is effectively calculated in the following two stages. First, the work is calculated which is spent to the generation of one elemental dislocation belonging to a wall of continuously distributed dislocations that is equivalent to a disclination dipole (Fig. 5) in the stress field of this dipole. At the second stage, the work spent to the generation of one elemental dislocation is integrated over all elemental dislocations that compose the wall of the continuously distributed dislocations. The integration procedure results in the work spent to the generation of the disclination dipole in its stress field. This work represents the energy W_s^Δ which, according to our two-stage calculations, is given as

$$W_s^\Delta = \frac{G\omega^2 a^2}{2\pi(1-\nu)} \left(1 + 2 \ln \frac{R}{2a} \right). \quad (18)$$

The energy of the interaction between the disclination dipoles W_{int}^Δ is calculated in a similar way. At the first stage, the work is calculated which is spent to the generation of one elemental dislocation belonging to a dislocation wall that is equivalent to one disclination dipole in the stress field created by another disclination dipole. Then the integration over all elemental dislocations composing the wall results in the work spent to the generation of one disclination dipole in the stress field of another dipole. With this calculation scheme, we find the energy W_{int}^Δ to be as follows:

$$W_{int}^\Delta = \frac{G\omega^2 a^2}{\pi(1-\nu)} \left\{ \left(1 + 2 \ln \frac{R}{2a} \right) \cos \alpha + (1 - \cos \alpha) \ln [2(1 - \cos \alpha)] \right\}. \quad (19)$$

Here α is the angle between the arms of the disclination dipoles (Fig. 6) which is assumed to be lower than $\pi/2$.

The energy $W_{int}^{\Delta-b2}$ of the interaction between a disclination dipole and structure 2 is calculated as the work spent to the generation of the wall of split dislocation configurations (Fig. 6) in the stress field of the disclination dipole. To do so, first, let us divide the wall of split dislocation configurations (each consisting of three partial dislocations, see Fig. 6) into the three (upper, intermediate, and lower) dislocation walls each consisting of periodically arranged partial dislocations, elements of the split dislocation configurations. Then we calculate the work spent to the generation of each the dislocation wall in the stress field created by the disclination dipole. In doing so, for the lower dislocation wall composed of partial dislocations with coordinates $(x=0, y=kh_2)$, where k is an integer, the work in question can be written as follows:

$$W_{int,1}^{\Delta-b2} = b \sum_{k=-\infty}^{+\infty} \int_0^{+\infty} \sigma_{xy}^\Delta(x, y=kh_2) dx, \quad (20)$$

where $\sigma_{xy}^\Delta(x, y)$ —the stress tensor component of the dipole of disclinations located at points $(0,0)$ and $(-x_1, y_1)$ —is given as²²

$$\sigma_{xy}^\Delta(x, y) = \frac{G\omega}{2\pi(1-\nu)} \left\{ \frac{xy}{x^2+y^2} - \frac{(x+x_1)(y-y_1)}{(x+x_1)^2+(y-y_1)^2} \right\}. \quad (21)$$

With the sum $\sum_{k=-\infty}^{+\infty}$ [figuring on the rhs of formula (20)] substituted under the integral sign and calculated, we have

$$W_{int,1}^{\Delta-b2}(x_1, y_1) = \frac{G\omega b}{2(1-\nu)h_2} \sin \frac{2\pi y_1}{h_2} \times \int_0^{+\infty} \frac{(x+x_1)dx}{\cosh \frac{2\pi(x+x_1)}{h_2} - \cos \frac{2\pi y_1}{h_2}}. \quad (22)$$

For the intermediate and upper dislocation walls composed of partial dislocations with coordinates $(x=0, y=p+kh_2)$ and $(x=0, y=2p+kh_2)$, respectively, the work under consideration can be calculated in the same way. In doing so, after some algebra, we obtain the following expressions that correspond to the intermediate and upper walls, respectively:

$$W_{int,2}^{\Delta-b2} = W_{int,1}^{\Delta-b2}(0, p) + W_{int,1}^{\Delta-b2}(x_1, y_1 - p), \quad (23)$$

$$W_{int,3}^{\Delta-b2} = W_{int,1}^{\Delta-b2}(0, 2p) + W_{int,1}^{\Delta-b2}(x_1, y_1 - 2p). \quad (24)$$

The summing of Eqs. (22)–(24) results in the following formula for the energy of the interaction between a disclination dipole and structure 2:

$$W_{int}^{\Delta-b2} = \frac{G\omega b}{2\pi(1-\nu)} \frac{h_2}{4\pi} \{ \Psi(0, \bar{p}) + \Psi(0, 2\bar{p}) + \Psi(\bar{x}_1, \bar{y}_1) + \Psi(\bar{x}_1, \bar{y}_1 - \bar{p}) + \Psi(\bar{x}_1, \bar{y}_1 - 2\bar{p}) \}, \quad (25)$$

where $\bar{x}_1 = 2\pi x_1/h_2$, $\bar{y}_1 = 2\pi y_1/h_2$, $\bar{p} = 2\pi p/h_2$, and

$$\Psi(a, b) = \sin b \int_a^{+\infty} \frac{t dt}{\cosh t - \cos b}. \quad (26)$$

The energy $W_{int}^{\Delta-vd}$ of the interaction between a disclination dipole and the virtual split dislocation configuration is effectively calculated as the work spent to the generation of this configuration in the stress field [given by formula (21)] of the disclination dipole:

$$W_{int}^{\Delta-vd} = -b \int_0^R \{ \sigma_{xy}^\Delta(x, y=0) + \sigma_{xy}^\Delta(x, y=p) + \sigma_{xy}^\Delta(x, y=2p) \} dx. \quad (27)$$

From Eq. (27) and the equations $x_1 = 2p \tan(\alpha/2)$ and $y_1 = 2p = 2a \cos(\alpha/2)$ (Fig. 6), we find

$$W_{int}^{\Delta-vd} = -\frac{G\omega b p}{2\pi(1-\nu)} \left(6 \ln \frac{R}{p} + \ln \frac{\cos^3(\alpha/2)}{8\sqrt{10-6\cos\alpha}} \right). \quad (28)$$

In the framework of our model, the disclination strength ω is related to geometric parameters of the defect structure as follows: $\omega \approx 3b/(4a) = 3b \cos(\alpha/2)/(4p)$. From this equation, with formulas (4), (12), (16), (18), (19), (25), and (28) substituted to Eq. (11), we find that the energy change associated with the transformation from structure 2 into the intermediate structure 2-3 is given as

$$\begin{aligned}
\Delta W_{2-3} \approx & \frac{Gb^2}{4\pi(1-\nu)} \left\{ -3Z_2 + 3 \ln \frac{R}{r_{0_2}} - 6[\eta_0 \coth \eta_0 - \ln(2 \sinh \eta_0)] + \frac{9}{4} \left[\cos^2 \frac{\alpha}{2} \left(1 + 2 \ln \frac{R \cos(\alpha/2)}{2p} \right) \right. \right. \\
& + \sin^2 \frac{\alpha}{2} \ln \left(4 \sin^2 \frac{\alpha}{2} \right) \left. \right] - 3 \cos \frac{\alpha}{2} \left(6 \ln \frac{R}{p} + \ln \frac{\cos^3(\alpha/2)}{8\sqrt{10-6\cos\alpha}} \right) - 4\Phi(\eta_0, \bar{p}) - 2\Phi(\eta_0, 2\bar{p}) \\
& + \frac{3h_2}{4\pi p} \cos \frac{\alpha}{2} [\Psi(0, \bar{p}) + \Psi(0, 2\bar{p}) + \Psi(2\bar{p} \tan(\alpha/2), 2\bar{p}) + \Psi(2\bar{p} \tan(\alpha/2), \bar{p})] \left. \right\} + W_{am} + \Gamma_{a/c} - 2(p - 2r_{0_2})\gamma,
\end{aligned} \tag{29}$$

where $\eta_0 = \pi r_{0_2}/h_2$, $\bar{p} = 2\pi p/h_2$, and functions $\Phi(\eta_0, t)$ and $\Psi(a, b)$ are given by formulas (17) and (26), respectively.

Now let us estimate the values of W_{am} , $\Gamma_{a/c}$, and γ , figuring on the rhs of Eq. (29). The difference of the energy density (per unit volume) between the amorphous and crystalline phases is estimated as follows:

$$w_{am} \approx \frac{G}{120(1-\nu)} \tag{30}$$

(see Ref. 23 and references therein). With w_{am} multiplied by $S [= 4p^2 \tan(\alpha/2)]$, the area of a triangle-like amorphous core section, we find W_{am} —the difference of the energy between the amorphous and crystalline phases—to be given as

$$W_{am} \approx \frac{Gp^2 \tan(\alpha/2)}{30(1-\nu)}. \tag{31}$$

Following estimates of Ref. 1, the stacking fault energy $\gamma \approx 7GB/[324\pi(1-\nu)]$.¹ The surface energy of the interface between the amorphous and crystalline phases is given as $\Gamma_{a/c} = \gamma_{a/c}L$, where $\gamma_{a/c}$ denotes the surface energy density (per unit area) of the interface, and L the perimeter of the amorphous dislocation configuration section. From Fig. 6 it follows that the perimeter $L = 4p\{\csc(\alpha/2) + \tan(\alpha/2)\}$. According to estimates (Ref. 24), the surface energy density is given as $\gamma_{a/c} \approx kGa$, where a denotes the mean interatomic distance in the amorphous phase, and k the nondimensional factor. As a corollary, we find

$$\Gamma_{a/c} \approx 4kGap\{\csc(\alpha/2) + \tan(\alpha/2)\}. \tag{32}$$

In metallic solids k ranges from 0.06 to 0.18.²⁴ In superconducting cuprates the surface energy of an interface between the isotropic amorphous phase and the highly anisotropic crystalline phase can be larger than that in metallic solids, in particular, due to the additional contribution caused by the difference in anisotropy between the amorphous and crystalline phases. That is, for high- T_c superconductors, values of k can be larger than those in metallic solids.

With the above estimates taken into account, the dependence of ΔW_{2-3} on tilt boundary misorientation θ was calculated with the help of formulas (29)–(32), for the follow-

ing values of parameters: $Z_2 \approx 1$, $R = (10^3 - 10^8)b$, $r_{0_2} \approx b$, $\alpha = \pi/20$, $k = 1/3$, $a \approx b$, and $p = 12b$. The results of our calculations indicate that $\Delta W_{2-3}(\theta) < 0$ in the range of θ ($\approx B/h_2$) from 5.5° to 7.1° ; see Fig. 7. According to these results, the formation of walls of amorphous dislocation configurations is more energetically favorable than that of walls of split dislocation configurations, if $5.5 \leq \theta \leq 7.1^\circ$. The numerically calculated dependence $\Delta W_{2-3}(\theta)$ has its minimum at $\theta \approx 7^\circ$ (Fig. 7); that is, the formation of walls of amorphous dislocation configurations is most favorable at $\theta \approx 7^\circ$. This is in a satisfactory agreement with experiments¹ that show such walls to exist at $\theta = 7.5^\circ$.

IV. CONCLUDING REMARKS

In this paper theoretical models have been suggested describing transformations of low-angle tilt boundaries (represented as walls of dislocation configurations) in high- T_c superconductors. In the framework of the models suggested, the conditions are theoretically revealed at which transformations of low-angle tilt boundaries are driven by a boundary energy release. So, it has been found that the transformation of a wall of perfect dislocations into a wall of split dislocation configurations is energetically favorable in the range of boundary misorientation θ from 0° to 7° ; this is in agreement with experimental data.¹ Also, according to our theoretical calculations (see Sec. III), the transformation of a wall of

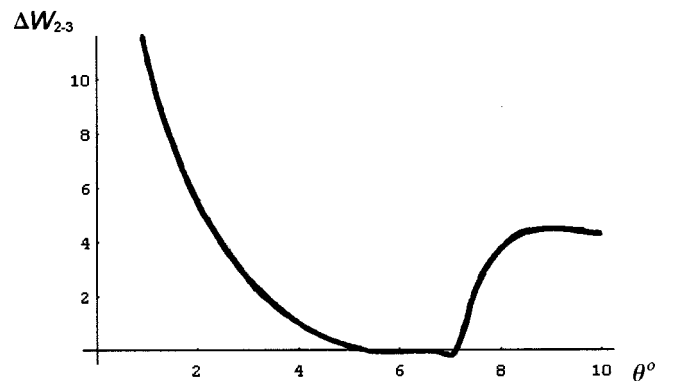


FIG. 7. Energy difference ΔW_{2-3} via tilt boundary misorientation angle θ . The energy values are given in units of $Gb^2/[4\pi(1-\nu)]$.

split dislocation configurations into a wall of amorphous dislocation configurations is energetically favorable in the range of θ from 5.5° to 7.1° , in which case the corresponding release of the energy reaches its maximum at $\theta \approx 7^\circ$. Low-angle tilt boundaries consisting of amorphous dislocation configurations have been experimentally observed at boundary misorientation $\theta \approx 7.5^\circ$;¹ this is in satisfactory agreement with theoretical constructs suggested here.

The critical current density J_c across low-angle tilt boundaries in high- T_c superconductors drastically decreases with boundary misorientation angle θ in the range from 0° to tentatively 15° .²⁻⁷ Current models^{8-10,12,17} of the grain-boundary effect on high- T_c superconductivity are based on the representation of low-angle tilt boundaries as walls of perfect dislocations [Fig. 1(a)]. However, in the light of both experiments¹ and theoretical analysis given in this paper, the transformations of low-angle tilt boundaries (Fig. 1) should be definitely taken into consideration of the effects of grain-boundary stress fields and core structures on high- T_c superconductivity. In particular, the Ginzburg-Landau formulation^{9,12} of the problem is worth being modified in the situation discussed (low-angle [100] tilt boundaries) in order to take into account contributions of split and amorphous dislocation configurations (Fig. 1) to the transport properties of low-angle tilt boundaries in high- T_c superconductors.

The Ginzburg-Landau-formalism-based description of the high- T_c superconducting properties of grain boundaries uses stress fields, chemical concentration fields, and electric charge density in vicinities of grain boundaries as an input. These fields modify the superconducting order parameter close to grain boundaries, cause the existence of hole depletion layers near grain boundaries and suppress the critical current densities J_c across grain boundaries.^{9,12-16,18} In general, the stress fields, the concentration fields, the electric charge density, and the grain-boundary core structure strongly influence each other. So, as it has been shown in this paper, the processes of formation of split and amorphized dislocations at low-angle tilt boundaries in high- T_c supercon-

ductors (Fig. 1) are driven by relaxation of stress fields (a release of the elastic energy density). The processes discussed (Fig. 1) initiate changes in concentration fields and electric charge distribution within and near grain boundaries. So, ions of different chemical elements in polyatomic cuprates exhibit different behaviors in response to stresses, in which case their concentration fields evolve in different ways with stress field changes that accompany the formation of split and amorphized dislocations (Fig. 1). Therefore the transformations of grain boundaries (Fig. 1) result in both redistribution of chemical elements and corresponding changes of the electric charge density in vicinities of such boundaries. In addition, the concentration fields and the electric charge densities are different in the dislocation cores and the bulk phase. As a corollary, the transformations of grain boundary dislocation cores (Fig. 1) result in both redistribution of chemical elements and corresponding changes of the electric charge-density field within and near core regions of low-angle tilt boundaries. A detailed (labor-consuming) analysis of the self-consistent changes of the grain-boundary core structure, the stress fields, the stoichiometric inhomogeneities and the electric charge density as well as their effects on the critical current density J_c across grain boundaries in high- T_c superconductors is beyond the scope of this paper. In any event, however, results of the models elaborated here can be effectively used as an input in further theoretical modeling (in particular, the Ginzburg-Landau-formalism-based description) of the transport properties of experimentally observed¹ low-angle tilt boundaries consisting of split and amorphous dislocation configurations.

ACKNOWLEDGMENTS

This work was supported, in part (for I.A.O.), by the Office of U.S. Naval Research (Grant No. N00014-99-1-0896) and the Russian Foundation of Basic Research (Grant No. 98-02-16075), and (for M.Yu.G. and I.A.O.) by the Volkswagen Foundation (Research Project No. 05019225).

*E-mail address: ovidko@def.ipme.ru

¹M. F. Chisholm and D. A. Smith, *Philos. Mag. A* **59**, 181 (1989).

²D. Dimos, P. Chaudhari, J. Mannhart, and F. K. LeGoues, *Phys. Rev. Lett.* **61**, 219 (1988).

³D. Dimos, P. Chaudhari, and J. Mannhart, *Phys. Rev.* **41**, 4038 (1990).

⁴Z. G. Ivanov, P.-Å. Nilsson, D. Winkler, J. A. Alarco, T. Claeson, E. A. Stepantsov, and A. Ya. Tzalenchuk, *Appl. Phys. Lett.* **59**, 3030 (1991).

⁵S. E. Russek, D. K. Lathrop, B. H. Moeckly, R. A. Buhrmann, and D. H. Shin, *Appl. Phys. Lett.* **57**, 1155 (1990).

⁶S. E. Babcock and J. L. Vargas, *Annu. Rev. Mater. Sci.* **25**, 193 (1995).

⁷M. Prester, *Supercond. Sci. Technol.* **11**, 333 (1998).

⁸M. F. Chisholm and S. J. Pennycook, *Nature (London)* **351**, 47 (1991).

⁹A. Gurevich and E. A. Pashitskii, *Phys. Rev. B* **57**, 13 878 (1998).

¹⁰D. Agassi, C. S. Pande, and R. A. Masumura, *Phys. Rev. B* **52**, 16 237 (1995).

¹¹D. M. Kroeger, A. Choudhury, J. Brynestad, R. K. Williams, R. A. Padgett, and W. A. Coghlan, *J. Appl. Phys.* **64**, 331 (1988).

¹²J. Betouras and R. Joynt, *Physica C* **250**, 256 (1995).

¹³H. Hilgenkamp, J. Mannhart, and B. Mayer, *Phys. Rev. B* **53**, 14 586 (1996).

¹⁴H. Hilgenkamp and J. Mannhart, *Appl. Phys. A: Mater. Sci. Process.* **64A**, 553 (1997).

¹⁵J. Mannhart, H. H. Hilgenkamp, and Ch. Gerber, *Physica C* **282-287**, 132 (1997).

¹⁶H. Hilgenkamp and J. Mannhart, *Appl. Phys. Lett.* **73**, 265 (1998).

¹⁷S. A. Kukushkin, I. A. Ovid'ko, and A. V. Osipov, *Tech. Phys. Lett.* **26**, 609 (2000).

¹⁸I. A. Ovid'ko (unpublished).

¹⁹N. D. Browning, E. M. James, K. Kyosuke, I. Arslan, J. P. Buban,

- J. A. Zaborac, S. J. Pennycook, Y. Xin, and G. Duscher, *Rev. Adv. Mater. Sci.* **1**, 1 (2000).
- ²⁰J. P. Hirth and J. Lothe, *Theory of Dislocations* (John Wiley, New York, 1982).
- ²¹I. A. Ovid'ko and A. B. Reizis, *J. Phys. D* **32**, 2833 (1999).
- ²²A. E. Romanov and V. I. Vladimirov, in *Dislocations in Solids*, edited by F. R. N. Nabarro (North-Holland, Amsterdam, 1992), Vol. 9, pp. 191–402.
- ²³R. C. Morris, *J. Appl. Phys.* **50**, 3250 (1979).
- ²⁴I. A. Ovid'ko, *Philos. Mag. Lett.* **79**, 709 (1999).